AD-779 516

FLUERICS 34: PLANAR-NOZZLE DISCHARGE COEFFICIENTS

Tadeusz M. Drzewiecki

Harry Diamond Laboratories
Washington, D.C.

September 1973

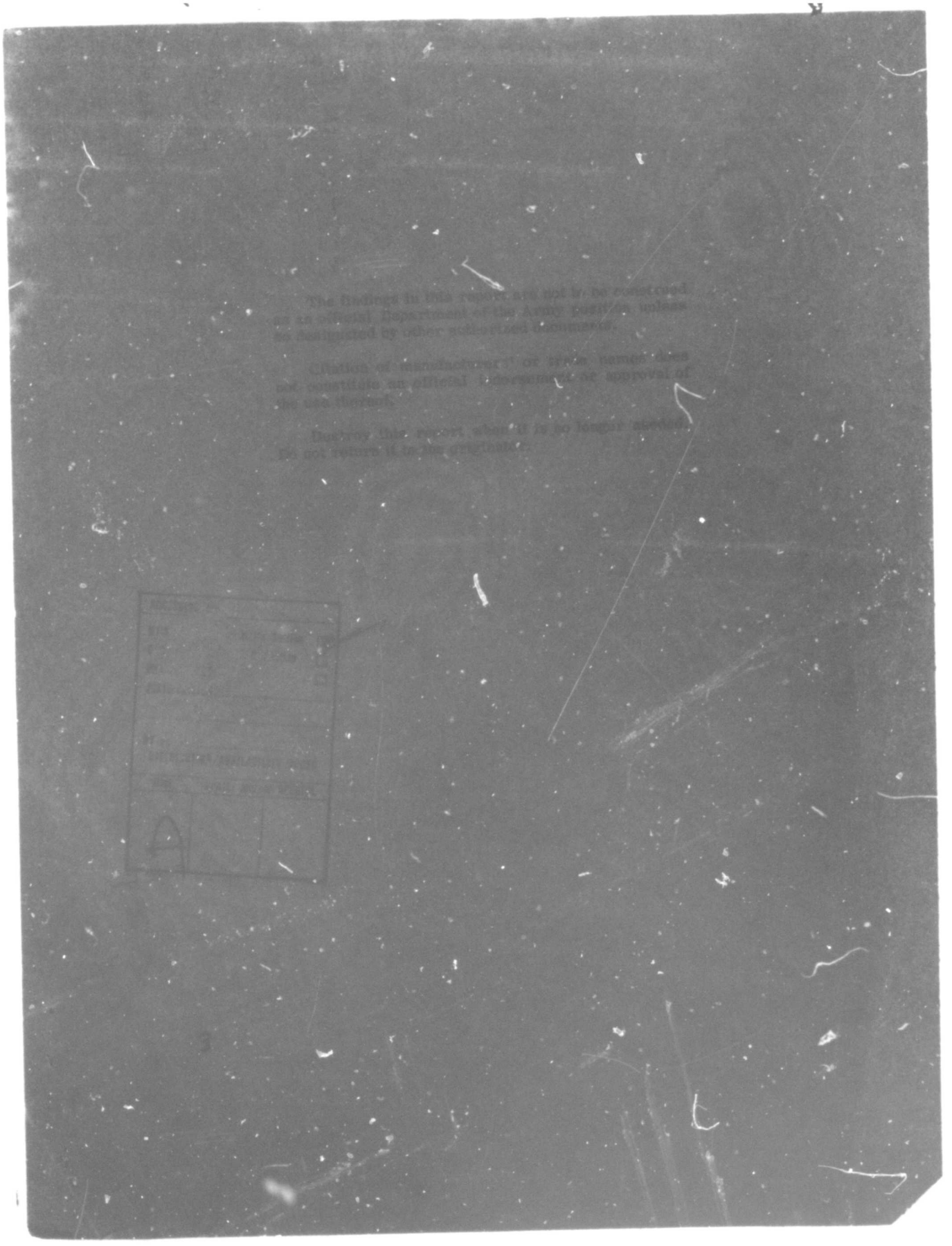

UNCLASSIFIED

Security Classification

AD779516

DOCUMENT CONTROL DATA - R & D

(Security classification of title, body of abstract and indexing annotation must be entered when the overall report is classified)

1. ORIGINATING ACTIVITY (Corporate author)

Harry Diamond Laboratories
Washington, D. C. 20438

2a. REPORT SECURITY CLASSIFICATION

Unclassified

2b. GROUP

3. REPORT TITLE

FLUERICS 34: PLANAR-NOZZLE DISCHARGE COEFFICIENTS

4. DESCRIPTIVE NOTES (Type of report and inclusive dates)

5. AUTHOR(S) (First name, middle initial, last name)

Tadeusz M. Drzewiecki

6. REPORT DATE	7a. TOTAL NO. OF PAGES	7b. NO. OF REFS
September 1973	~~36~~ 37	8

8a. CONTRACT OR GRANT NO.	9a. ORIGINATOR'S REPORT NUMBER(S)
b. PROJECT NO. DA-1T061102A33B	HDL-TM-72-33
c. AMCMS Code: 611102.11.711200	9b. OTHER REPORT NO(S) (Any other numbers that may be assigned this report)
d. HDL Proj: 302331	

10. DISTRIBUTION STATEMENT

Approved for Public Release: Distribution Unlimited

11. SUPPLEMENTARY NOTES	12. SPONSORING MILITARY ACTIVITY
	Army Materiel Command

13. ABSTRACT

This report deals with the formulation of a general expression for calculating planar-nozzle discharge coefficients c_d. The expression is in terms of constants whose values depend only on geometry and are directly calculable from a simple solution of the Karman-Pohlhausen momentum integral equations. The assumption of one-dimensional, inviscid flow to determine the free-stream velocities and pressure distributions is shown to be valid by the good agreement with observation. Measured and theoretically determined discharge coefficients for nozzles of widths from 0.5 to 2.0 mm generally agree to within 4 percent. This is excellent in light of the fact that the normal experimental deviation is about 4 percent. The discharge coefficient c_d remains virtually constant for turbulent flow. For the case where transition occurs in the inlet tubing to the nozzle, experimental values of transition Reynolds number and turbulent discharge coefficients are in excellent agreement with theory. In order to facilitate use of these results as a design guide, the analytical expression for c_d is graphed for various nozzle geometries to include variations in aspect ratio, throat straight section, and contraction ratio. The simplicity of solution allows a simple program on a programmable calculator to give the desired discharge coefficients for most nozzle configurations. In general, a nozzle with an aspect ratio of two, contraction ratio, and contraction length ratio of ten has a discharge coefficient $c_d > 0.9$ for $Re > 2500$.

DD FORM 1 NOV 68 1473 REPLACES DD FORM 1473, 1 JAN 64, WHICH IS OBSOLETE FOR ARMY USE.

UNCLASSIFIED

Security Classification

1

14. KEY WORDS	LINK A		LINK B		LINK C	
	ROLE	WT	ROLE	WT	ROLE	WT
Fluidics						
Fluerics						
Flow						
Discharge						
Coefficients						
Nozzle						
Planar Nozzles						
Transition						

AD

DA-1T061102A33B
AMCMS Code: 611102.11.71200
HDL Proj: 302331

HDL-TM-72-33

FLUERICS 34: PLANAR-NOZZLE DISCHARGE COEFFICIENTS

by

Tadeusz M. Drzewiecki

September 1973

U.S. ARMY MATERIEL COMMAND
HARRY DIAMOND LABORATORIES
WASHINGTON, D.C. 20438

4

TABLE OF CONTENTS

LIST OF ILLUSTRATIONS

1. INTRODUCTION

With the advent of the fluidics technology in 1959 the area of miniature fluid mechanics has become a field of great interest. Major parts of a fluid amplifier geometry are the planar nozzles, which form the supply jet and also the control (interaction) jets that deflect the supply jet. In order to predict the input/output operating characteristics of fluid amplifiers accurately the respective input impedances must be known. The discharge coefficient describes the viscous losses in a nozzle and as such determines the nozzle's impedance to flow. Typical nozzles used in fluid amplifier applications are 0.5 mm wide and consequently operate at a fairly low Reynolds number, usually not exceeding 2×10^4. The flow in the nozzles themselves is therefore generally laminar, although the jets outside may become turbulent.

In the past, most analytical consideration of discharge coefficients has been limited to the axisymmetric cases used in flow metering. These discharge coefficients and the standard nozzle designs are given in the ASME Report on Fluid Meters[1]. It has been well known that the presence of viscous forces at the walls causes the flow to slow down, thus decreasing the amount of flow that can be passed at a given pressure difference across the nozzle. Simmons[2] assumed arbitrary velocity profiles within the nozzle and calculated the displacement thickness and, hence, the discharge coefficient for axisymmetric nozzles at high Reynolds number. Williams and Smetana[3] used the concept of displacement thickness and the Karman-Pohlhausen momentum integral equation to calculate a two-dimensional nozzle discharge coefficient. However, they used just one nozzle configuration of a single constant radius of curvature where the flow was accelerated from a constant cross-section plenum through a converging section made up of two quarter circles. McRee[4] verified Williams and Smetana's (ref 3) theory for the one particular nozzle. McRee and Moses[5] analyzed aspect ratio or the effect of nozzle height. Although they calculated only the displacement thickness and applied the results to turbulent jet reattachment, there was good agreement between theory and experiment.

---

[1] FLUID METERS, Their Theory and Application, Report of ASME Research Committee on Fluid Meters, 5th edition, 1959

[2] Simmons, F.S., "Analytic Determination of the Discharge Coefficients of Flow Nozzles," NACA TN 3447, Lewis Flight Propulsion Labs, Cleveland, Ohio, April 1955

[3] Williams, J.C. and F.O. Smetana, "Theoretical Study of a Convergent Nozzle and Free Jet Flow," Proceedings of the Fluid Amplification Symposium, Harry Diamond Laboratories, Vol. 1, October 1965

[4] McRee, D.I., "Experimental Study of a Convergent Nozzle and Free Jet Flow," Proceedings of the Fluid Amplification Symposium, Harry Diamond Laboratories, Vol. 1, October 1965

[5] McRee, D.I. and H.L. Moses, "The Effect of Aspect Ratio and Offset on Nozzle Flow and Jet Reattachment," Advances in Fluidics, edited by F.T. Brown, presented at 1967 ASME Fluidics Symposium, Chicago, Illinois, May 1967

Based on the above cited work, this author has generalized the theory so that it can be applied to virtually any kind of varying cross-section conduit, especially planar nozzles, e.g., converging walls confined between two parallel planes. The following sections give a general mathematical formulation, specific calculations, experimental comparisons, and design criteria in the form of graphs of c_d versus Re for various geometric conditions.

2. ANALYSIS

2.1 General Formulation

The accepted definition of discharge coefficient, c_d, is the ratio of actual flow to ideal one-dimensional inviscid flow through a conduit, in this case, a nozzle or orifice.

$$c_d = \frac{Q_a}{Q_i} \tag{1}$$

By assuming a one-dimensional inviscid flow as the ideal flow and applying the Bernoulli equation, (1) becomes

$$c_d = \frac{Q_a}{A\sqrt{\frac{2\Delta P}{\rho}}} \tag{2}$$

where:

Q_a = actual flow

Q_i = ideal flow

A = exit area of nozzle

ΔP = difference between nozzle stagnation pressure and exit static pressure

ρ = fluid density

The laminar flow of a fluid in the proximity of a solid boundary is characterized by a layer of slowly moving fluid in the immediate vicinity of the boundary and a free stream of higher velocity. This boundary layer effect is shown in figure 1. A boundary layer thickness, δ, is defined as the perpendicular displacement from the surface to where the fluid velocity is 99 percent

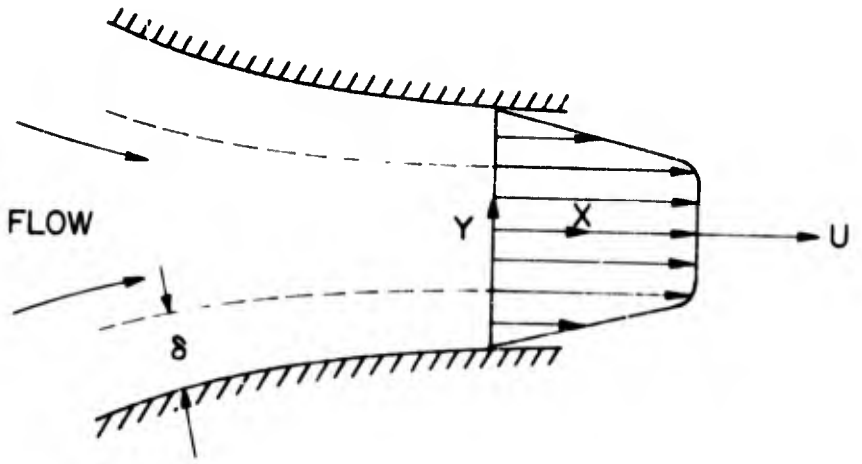

Figure 1. Boundary layer effect in the proximity of a wall.

of the free-stream velocity. The displacement thickness, δ^*, (p. 122, Schlichting[6]) is the distance a wall must be displaced toward the free-stream so that the uniform flow between some point Y and the displaced wall is equal to the actual flow from that same point Y to the actual wall position. This effect is illustrated in figure 2. The net effect then of the boundary layer is to decrease the effective area through which the ideal flow can pass. This effective reduction in area gives rise to a general expression for the discharge coefficient so that, neglecting three-dimensional effects (corner effects):

$$c_d = \frac{Q_a}{Q_i} = \frac{U A_{eff}}{U A_{actual}} = \frac{A_{eff}}{A_{actual}} \tag{3}$$

or

$$c_d = \frac{(w - 2\delta^*_1)(h - 2\delta^*_2)}{wh} = \left[1 - 2\delta^*_1/w\right]\left[1 - 2\left(\delta^*_2/w\right)(w/h)\right] \tag{4}$$

[6]Schlichting, H., Boundary Layer Theory, McGraw-Hill, New York, 4th edition, 1960, pp. 122, 244, 247, 251, 413.

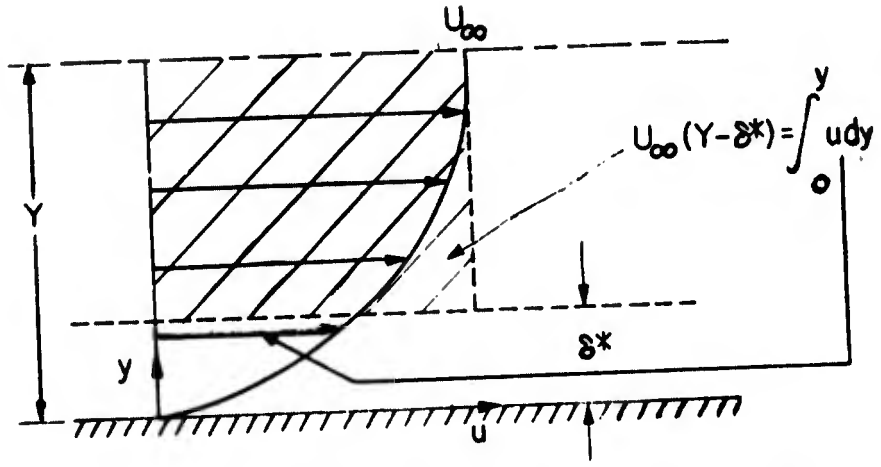

Figure 2. A physical description of displacement thickness.

where

$$A_{eff} = (w - 2\delta^*_1)\ (h - 2\delta^*_2)$$

$$A_{actual} = wh$$

U = ideal velocity = $\sqrt{\frac{2\Delta P}{\rho}}$

$\frac{h}{w}$ = aspect ratio; nozzle height/nozzle width

δ^*_1 = displacement thickness for contracting walls

δ^*_2 = displacement thickness for plane walls

By postulating a fourth-order polynomial for the velocity distribution in the boundary layer, a unique relationship exists between the displacement thickness, δ^*, and the momentum thickness, θ. (This is given in Schlichting's equation 12.31, ref 6.)

$$\frac{\delta^*}{\theta} = \frac{\frac{3}{10} - \frac{1}{120}\Lambda}{\frac{37}{315} - \frac{1}{945}\Lambda - \frac{1}{9072}\Lambda^2} \qquad (5)$$

where:

θ = momentum thickness $\equiv \int_0^Y \frac{u}{U}\left(1 - \frac{u}{U}\right) dy$

$\Lambda = \frac{\delta^2}{\mu U}\left(-\frac{dp}{dx}\right)$

μ = fluid viscosity

δ = boundary layer thickness; $\frac{\delta^*}{\delta} = \frac{3}{10} - \frac{1}{120}\Lambda$

U = potential free stream velocity

$\frac{dp}{dx}$ = free stream pressure gradient

Momentum thickness, it is recalled, is defined in much the same manner as is displacement thickness. This can be visualized easily by noting that the sum of the displacement and the momentum thickness is the distance a wall must be moved up in order that the momentum flux of a uniform stream be equal to the momentum flux of the actual flow over the actual wall. Note here particularly that the assumption of zero-pressure gradient at a nozzle exit reduces equation 5 to: $\delta^*/\theta = 2.554$.

If the free-stream velocity at the edge of the boundary layer can be described as a continuous function of the downstream coordinate (s, along a contracting wall, x, along the nozzle axis), then a solution of the Karman-Pohlhausen momentum integral equation can be obtained. From this solution, the momentum thickness can be expressed in terms of a simple quadrature. (equation 12.37 of ref 6). Normalizing by U_∞ rather than U, this expression becomes

$$\frac{U_\infty \theta^2}{w\nu} = \frac{0.47}{\left[\frac{U\left(\frac{x}{w}\right)}{U_\infty}\right]^6} \int_0^{x/w} \left[\frac{U(\chi)}{U_\infty}\right]^5 d(\chi) \qquad (6)$$

where:

U_∞ = nozzle exit (maximum) velocity

θ = momentum thickness at x/w

w = nozzle width

ν = kinematic viscosity

χ = integration variable for downstream distance = x/w

U = free-stream velocity as a function of x/w

x = downstream coordinate, measured from the point where the boundary layer originates

At the nozzle exit, the ratio U/U_∞ on the outside of the integral becomes unity, so that

$$\frac{U_\infty \theta^2 \Big|_{exit}}{w\nu} = 0.47 \int_0^{x/w \Big| exit} \left[\frac{U(\chi)}{U_\infty}\right]^5 d(\chi) \tag{7}$$

From the assumption of a zero exit static pressure gradient, using equation 5 one obtains

$$\frac{\delta^*}{w} = 2.554 \left\{ \frac{0.47 \int_0^{x/w \Big| exit} \left[\frac{U(\chi)}{U_\infty}\right]^5 d(\chi)}{Re_{exit}} \right\}^{1/2} \tag{8}$$

where:

Re_{exit} = Reynolds number based on nozzle width = $U_\infty w/\nu$

The expression in the integral of equation 8 is a function only of geometry if an expression exists relating free-stream velocity to geometry. If the integral is a constant for a given geometry, then the expression for c_d,

(equation 4), can be rewritten in terms of the nozzle exit Reynolds number Re, the aspect ratio, h/w, and two geometry dependent constants D_1 and D_2 so that

$$c_d = \left[1 - \frac{2D_1}{\sqrt{Re}}\right]\left[1 - \frac{2D_2}{\frac{h}{w}\sqrt{Re}}\right] \tag{9}$$

Equation 9 will hold, then, for any flow conditions where the flow is not fully developed or when any of the boundary layers have not met. Corrections can be made if it is determined that one set of boundary layers has met. If no correction is made, it is expected that the theory will underestimate c_d to some degree since physically $\lim_{Re \to 0} c_d = 0$, but when c_d from equation 9 is zero, $Re > 0$. A similar expression can be obtained for a momentum flux discharge coefficient. This decrement in jet momentum flux may affect the calculation of jet deflection in fluid amplifiers, and can be determined by adding the momentum thickness to the displacement thickness in equation 4.

2.2 Formulation for Continuous Cross Sections

The simplest formulation for the free-stream velocity is one-dimensional inviscid flow.

Consider the case of planar nozzles having a converging section made up of contoured walls sandwiched between two parallel plates (fig. 3). The two sets of boundary layers of concern are the set on the plates and the set on the converging walls. In general, incompressible flow in a converging section is accelerated and the boundary layer thickness is decreased. This effect is shown schematically in figure 4. By assuming a uniform velocity across the nozzle, one obtains from continuity that

$$hU(x)Y(x) = whU_\infty$$

or

$$\frac{U}{U_\infty}\left(\frac{x}{w}\right) = \frac{w}{Y\left(\frac{x}{w}\right)} \tag{10}$$

Thus, the velocity is seen to be proportional to the reciprocal of the local width of the nozzle. This velocity can be assumed to be the free-stream velocity in calculating the displacement thickness for the boundary layer on the plane top and bottom walls. For the curved walls, however, the velocity cannot be in the x direction as obtained from equation 10. The converging wall makes an

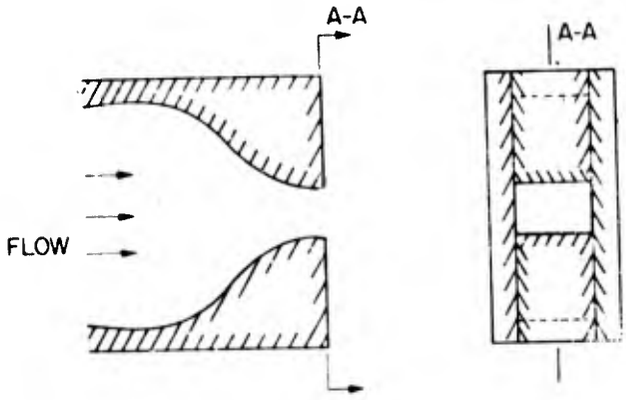

Figure 3. Schematic of a planar nozzle.

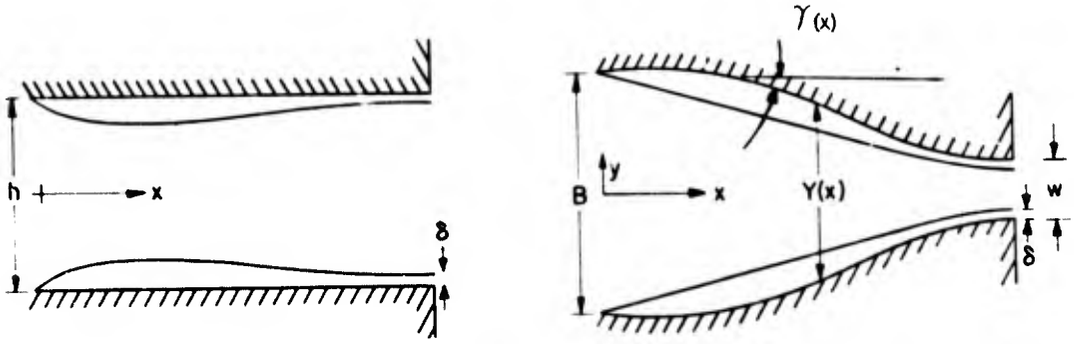

Figure 4. Boundary layer growth in a planar nozzle.

angle γ with the x direction, as shown in figure 4, so that in the vicinity of the converging wall the free-stream velocity is higher than the mid-plane velocity. The free-stream velocity at the edge of the curving boundary layer is thus

$$\frac{U\left(\frac{x}{w}\right)}{U_\infty} = \frac{1}{\frac{Y\left(\frac{x}{w}\right)}{w} \cos \gamma} \tag{11}$$

This latter relationship will hold only when $\cos \gamma > 0$, so that geometries where γ is near $\pi/2$ are disallowed. Wall angles of greater than 1.25 rad (72 deg) have from experience been found to be too abrupt for equation 11 to hold. Such would be the case in an abrupt change in area, or two quadrants

of a circle joined at the $\pi/2$ point as shown in figure 5. When the nozzle geometry is known, then the integral in equation 8 can be evaluated and c_d may be determined.

Consider, therefore, a nozzle consisting of a straight section, a converging section composed of two tangent circular arcs and another straight section as shown in figure 6. The boundary layer integral for the parallel plates of equation 8 reduces to

$$\int_0^{x/w} = \frac{L_1/w}{(B/w)^5} + L_2/w + \int_0^{\alpha} \left[\frac{(R_1/w)\cos\beta}{\left[(B/w) - 2\,(R_1/w)\,(1 - \cos\beta)\right]^5} + \frac{(R_2/w)\cos(\alpha - \beta)}{\left[1 + 2\,(R_2/w)\left(1 - \cos\left[\alpha - \beta\right]\right)\right]^5} \right] d\beta \qquad (12)$$

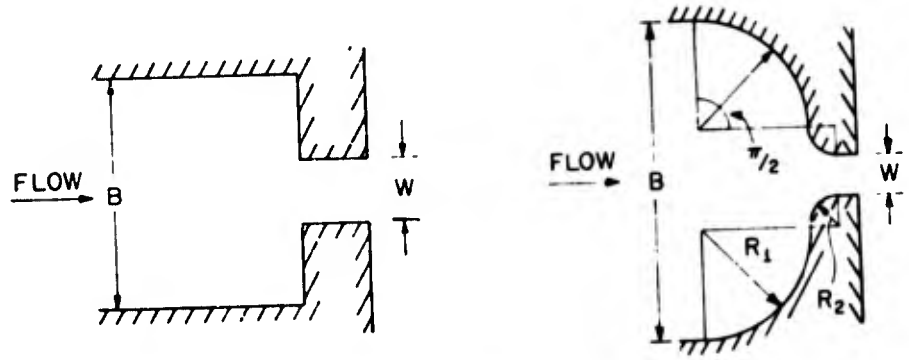

Figure 5. Nozzles where the cross-sectional area change is discontinuous.

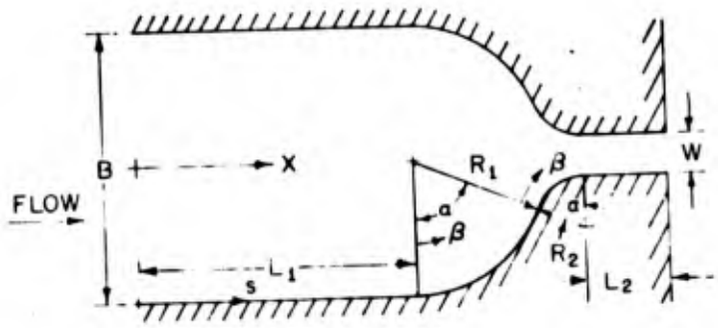

Figure 6. A smooth double-arc-of-a-circle nozzle.

and the integral for the contracting walls reduces to

$$\int_0^{s/w} = \frac{\frac{L_1}{w}}{\left[\frac{B}{w}\right]^5} + \frac{L_2}{w} + \int_0^{\alpha} \left\{ \frac{\frac{R_1}{w}}{\left[\left[\frac{B}{w} - 2\,\frac{R_1}{w}\,(1 - \cos\beta)\right]\cos\beta\right]^5} + \frac{\frac{R_2}{w}}{\left[\left[1 + 2\,\frac{R_2}{w}\,(1 - \cos(\alpha - \beta))\right]\cos(\alpha - \beta)\right]^5} \right\} d\beta \qquad (13)$$

where β is the angle measured in the direction of flow from the start of curvature (fig. 6). In the usual case

$$\left[\frac{B}{w}\right]^5 \gg \frac{L_1}{w}$$

so that the length of plenum has little or no effect on c_d (see also Simmons, ref 2), whereas, the length of straight section downstream of the convergence, L_2/w has a great influence on c_d. Equations 12 and 13 are very simply programmable either on a digital computer or even on a desk-top programmable calculator.

In general, if there is no discontinuity (abrupt change in area) as in figure 5a, equation 12 can be used to calculate the displacement thickness on the parallel walls; this is not true, however, with equation 13, becuase cos α may become zero.

Considering the type of nozzle examined by Williams and Smetana (ref 3) shown in figure 7, if the converging section is a quadrant of a circle, then one may use the free-steam function along the curved wall that they used.

$$\frac{U}{U_\infty} = \sin^2\beta \tag{14}$$

Equation 14 is then used in lieu of equation 11. The integral of equation 8 becomes

$$\int_0^{s/w} = \frac{\frac{L_1}{w}}{\left[\frac{B}{w}\right]^5} + \frac{R}{w}\int_0^{\pi/2} \sin^{10}\beta \; d\beta + \frac{L_2}{w}$$

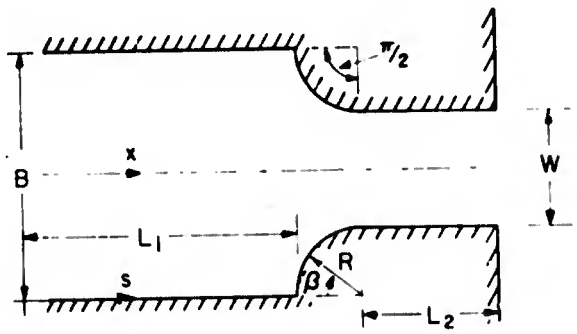

Figure 7. A single radius-of-curvature nozzle.

and evaluating becomes

$$\int_0^{s/w} = \frac{\frac{L_1}{w}}{\left[\frac{B}{w}\right]^5} + 0.38656\,\frac{R}{w} + \frac{L_2}{w} \tag{15}$$

Equation 15 in conjunction with equation 12, with $R_1 = 0$ and $\alpha = \pi/2$ can be used to solve for this nozzle-discharge coefficient.

2.3 Formulation for Abrupt Change in Cross Section

A slightly more complicated form for the velocity distribution at the boundary layer edge must be assumed in the case of abrupt change-of-area nozzles, such as that shown in figure 8. If one considers the flow upstream of the constant-radius nozzle, the flow field is basically a sink flow, as shown in figure 8, so that the velocity along the straight wall in the s direction becomes

$$\frac{U\left[\frac{s}{w}\right]}{U_\infty} = \frac{1}{\pi\left[\frac{1B}{2w} - \frac{s}{w}\right]} \tag{16}$$

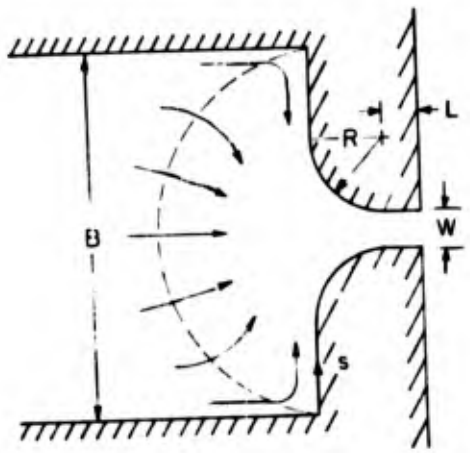

Figure 8. An abrupt change-of-area nozzle.

In the region of the nozzle along the curved wall, the flow is much like the flow in the single radius of curvature nozzle described in the previous section; in other words, a second-order periodic function. Maintaining a continuous velocity in s/w by matching the velocity and gradient at both the beginning of the curvature and at the nozzle exit (so that

$$U\Big|_{exit} = U_\infty, \quad \frac{dU}{dy}\Big|_{exit} = 0),$$

the velocity distribution is thus

$$\frac{U\left[\frac{s}{w}\right]}{U_\infty} = \frac{1}{\pi\left(\frac{R}{w} + \frac{1}{2}\right)}\left[\cos^2\beta + \frac{\frac{R}{w}}{\frac{R}{w} + \frac{1}{2}}\sin\beta\,(1 - \sin\beta)\right] + \sin^2\beta \quad (17)$$

the integral in equation 8 can be written as:

$$\int_0^{s/w} = \frac{1}{4\pi^5}\left(\frac{1}{\left(\frac{R}{w} + \frac{1}{2}\right)^4} - \frac{16}{\left(\frac{B}{w}\right)^4}\right) + \int_0^{\pi/2} \frac{R}{w}\left[\frac{1}{\pi\left(\frac{R}{w} + \frac{1}{2}\right)}\left[\cos^2\beta + \frac{\frac{R}{w}}{\frac{R}{w} + \frac{1}{2}}\sin\beta\,(1 - \sin\beta)\right] + \sin^2\beta\right]^5 d\beta + \frac{L}{w} \quad (18)$$

The velocity at the edge of the parallel plate boundary layer, however, cannot be considered from a sink-flow point of view. This was determined after first considering it as such and then not being able to verify it experimentally. Experiments indicated that the velocity distribu n along the nozzle axis can be represented best by simply considering that the flow is through a nozzle of a converging section as described in the beginning of section 2.2 and shown in figure 6. The first radius of curvature is given as one-half the plenum width, minus the second radius, minus half the nozzle width, or

$$\frac{R_1}{w} = \frac{1}{2}\frac{B}{w} - \frac{R_2}{w} - \frac{1}{2} \quad (19)$$

This may be explained by consideration of the expected streamline pattern in an abrupt change in area nozzle as shown in figure 9. By replacing streamline 1 with a wall, the nozzle, as far as the center-line velocity is concerned, now has the flow pattern of a smoothly converging nozzle. Thus, the integral of equation 8 for the plate boundary layers can be replaced by equation 12, using equation 19 for R_1/w and using $\alpha = \pi/2$.

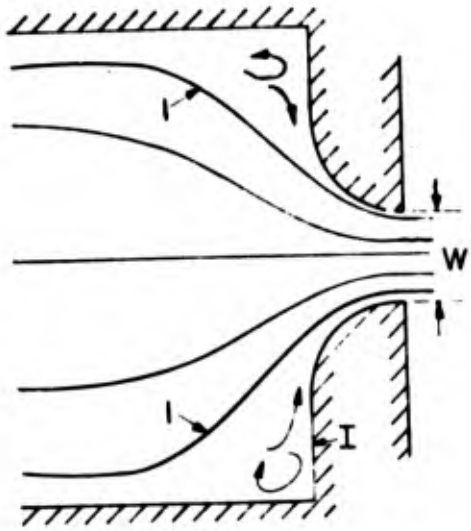

Figure 9. Probable streamline configuration in an abrupt change-of-area nozzle.

2.4 Transition to Turbulence

When the flow in a nozzle is turbulent, the discharge coefficient is constant over a large range of Reynolds numbers. It is therefore of great interest to determine when turbulence may occur in the nozzle.

If there are no upstream disturbances and only the stability of the boundary layer in the nozzle is considered, then the flow will probably become turbulent starting at the nozzle exit, at the point of minimum favorable pressure gradient.

Schlichting (ref 6, p. 410) indicates that the critical Reynolds number for a zero-pressure gradient is 420, based on displacement thickness. This is determined from a stability analysis of the Blasius profile as opposed to the approximate polynomial of the momentum integral method, where a value of

645 is obtained. Using the value for critical Reynolds number of 420 and transforming it to a Reynolds number based on nozzle width gives

$$Re_{crit} = \frac{1.764 \times 10^5}{D_1^2} \tag{20}$$

where

D_1 = constant derived from nozzle geometry in equation 9.

From previous experience, D_1 is known to generally range in the order of from 1.0 to 5.0. Thus, the range for critical Reynolds number based on the instability of the laminar boundary layer within the nozzle is

$$7.0 \times 10^3 \leq Re_{crit} \leq 1.764 \times 10^5$$

For the usual case of $D_1 \simeq 2$, Re_{crit} is then of the order of 4×10^4. In fluid amplifier applications or other applications where the nozzles are of the order of 0.5 mm, the Reynolds number rarely exceeds 2×10^4; thus, one would not normally expect this mode of transition to turbulence when considering small nozzles. It should be noted, however, that for long slender nozzles, D_1 may exceed 2.0 and even approach 5.0 so that this mode should not be discounted until the operating range is determined.

A far more likely reason for the flow to become turbulent at low Reynolds numbers is that upstream disturbances are grea', or that the flow entering the plenum has already become turbulent.

In this case, consider that a nozzle is supplied with fluid from a circular tube of sufficient length, so that the flow in the tube is always fully developed. In such an event, when the tube Reynolds number based on diameter and mean velocity exceeds 2300, the entering flow into the nozzle will already be turbulent; hence, the flow in the nozzle should behave differently. The critical Reynolds number based on nozzle width and average velocity then becomes

$$Re_{q\ crit} = 575\,\pi\,\frac{d}{h} \tag{21}$$

where

Re_q = Reynolds number based on nozzle width and average velocity

d = tubing inside diameter

h = nozzle height

When the ratio of pipe diameter to nozzle height is of the order of 1.0, the critical nozzle Reynolds number is about 1800.

There is yet another mode of transition to turbulence when the fluid enters the plenum of the nozzle through a bounding plate (not along the flow axis). The resultant stagnation flow may become unstable if an adverse pressure gradient is allowed to exist. This will occur when the cross-sectional area of the inlet fitting or tubing is less than that of the curtain area (fig. 10), and also if the curtain area is less than the plenum cross-sectional area. The effect is that of a diffusing flow, which is far less stable than that of the accelerating flow. There is no method presented for determination of the stability of such a flow field; but since the effects are definitely deleterious, care should be taken to maintain a decreasing set of areas from inlet to plenum.

3. EXPERIMENTAL VERIFICATION

The following section is in three parts, the first verifies the validity of the one-dimensional velocity assumption, the second compares the theoretical and experimental values of discharge coefficient for laminar flow, and the third verifies the second transition to turbulence hypothesis of section 2.3.

3.1 Experimental Verification of the One-Dimensional Flow Assumption

Static pressure measurements were made along the axis of four nozzles. In every case considered, the working fluid was air at room temperature (24°C).

The first nozzle (fig. 7) of single radius of curvature equal to 10 nozzle widths had an aspect ratio of 1.0. The velocity was determined from the distribution used in the integral in equation 12, with $R_1 = 0$, and $\alpha = \pi/2$. The static pressure was theoretically determined by equation

$$\frac{P}{P_+} = 1 - \left[\frac{U}{U_\infty}\right]^2$$

Figure 11 shows good agreement between theory and experiment. The results for two supply stagnation pressures (two representative Reynolds numbers) show similarity as expected, and also demonstrate that the theory is valid in the operating range of most fluid amplifiers.

The second nozzle consisted of an abrupt change-of-area nozzle and the third was a smooth change-of-area nozzle, made by modifying the former nozzle with clay so that the initial radius of curvature R_1 would conform to equation 19. If the assumption made in section 2.2 is valid, the theoretical results should be the same for both nozzles. The experimental results are found to be almost identical. The comparison between experiment and theory can be seen in figure 12.

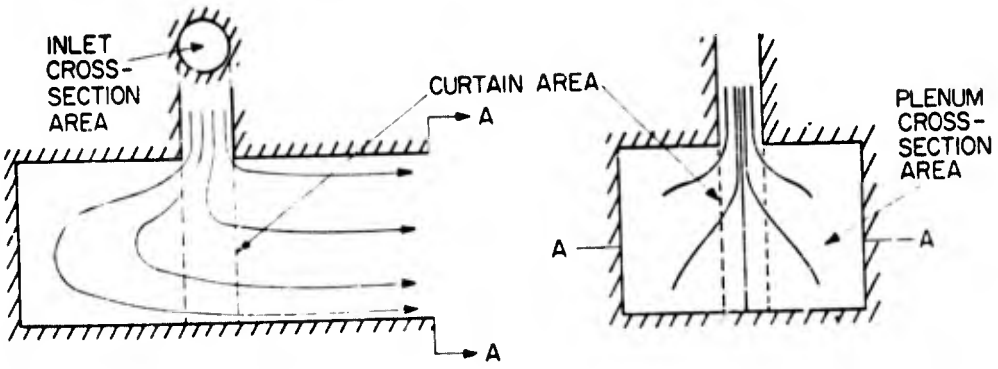

Figure 10. Stagnation flow entering a plenum.

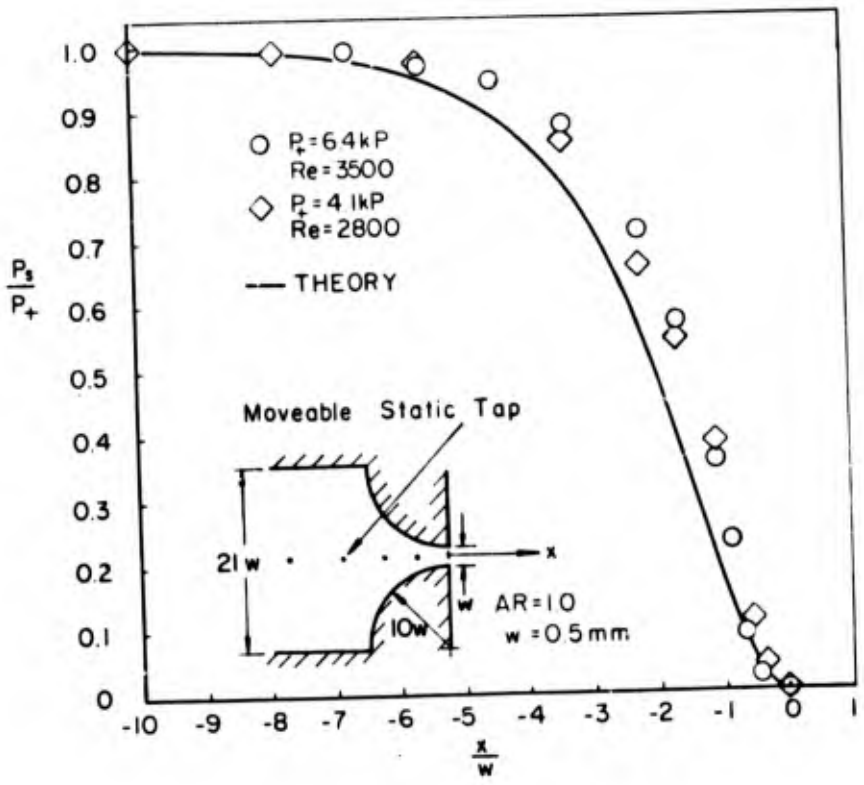

Figure 11. Axial static pressure distribution in a single radius-of-curvature nozzle.

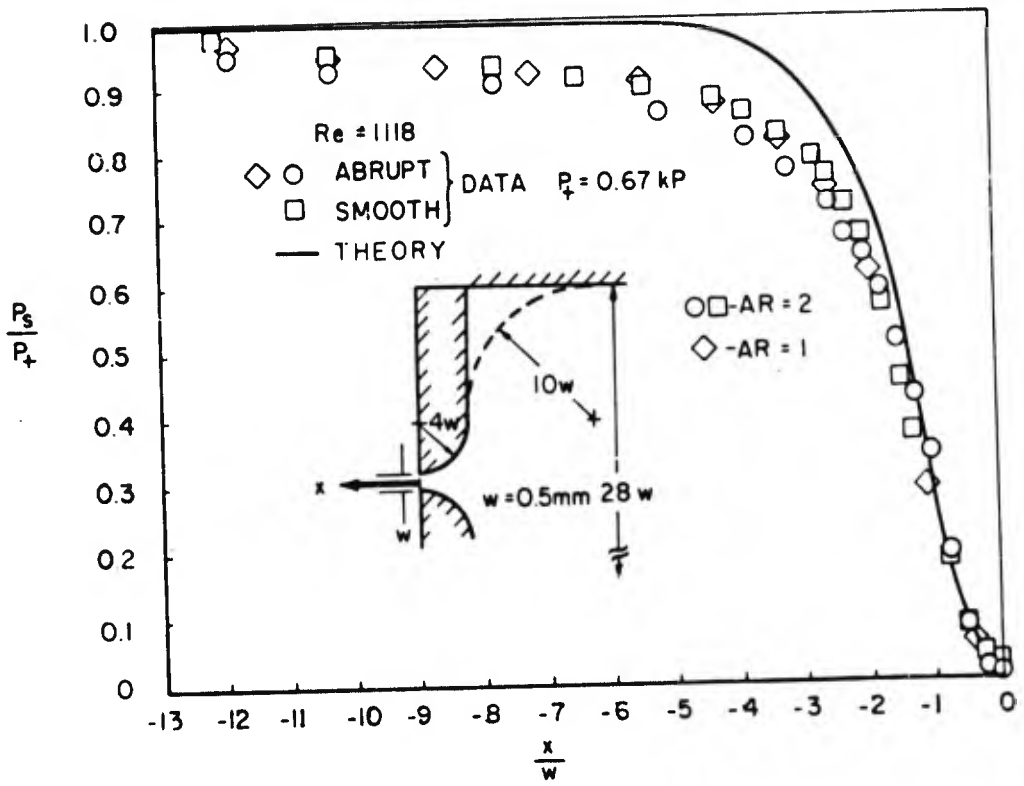

Figure 12. Axial static pressure distribution in an abrupt change-of-area and modified smooth nozzle.

The only discrepancy between theory and experiment occurs well inside the plenum. The highly accelerated portion of the flow is well represented by the theory as shown by the good agreement in the region within three nozzle widths of the exit. Not only are the pressure profiles similar in Reynolds number, but also in aspect ratio. This is to be expected as long as opposite pairs of boundary layers have not met and there is a free stream corresponding to an inviscid flow.

The fourth nozzle had a smoothly changing cross section of the type first discussed in section 2.1. The geometry, as well as the comparison between theory and experiment, is given in figure 13.

The overall agreement is fairly good and especially good in the highly accelerated region. Note, however, that while the pressure is basically constant in the plenum, it is not quite so in the straight section at the end of the contraction. The two representative Reynolds numbers used again show the similarity of the flows.

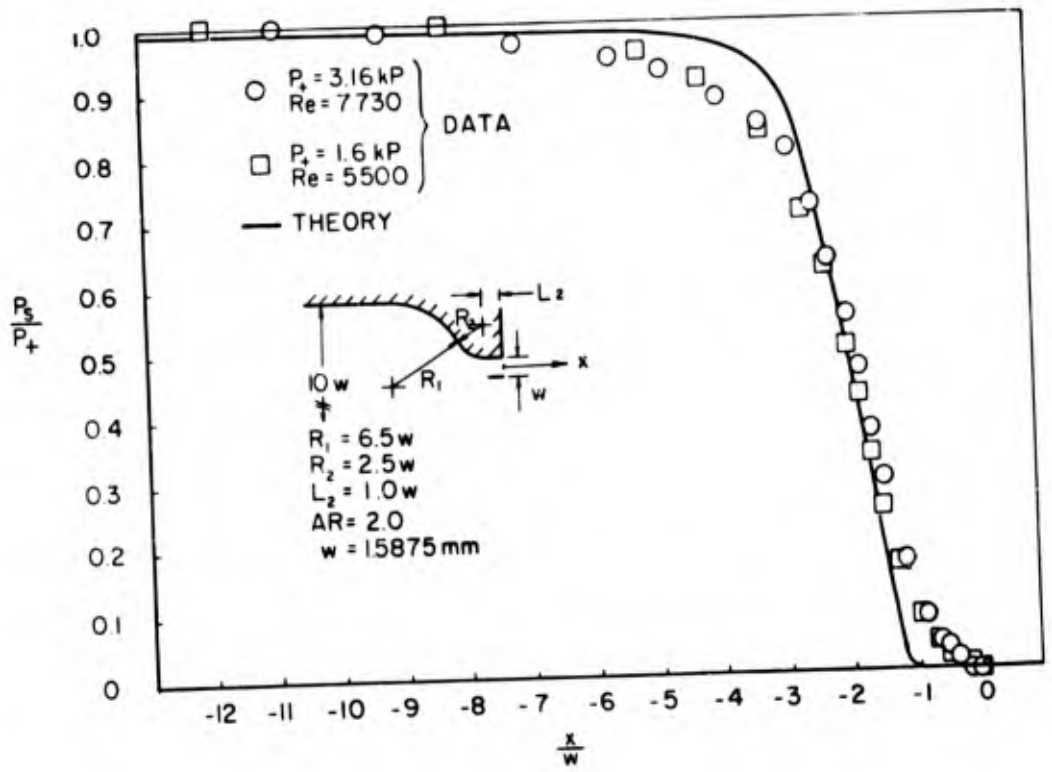

Figure 13. Axial static pressure distribution in a smooth double-arc-of-a-circle nozzle.

In all the above comparisons, the exit pressure gradient was found to be virtually if not exactly zero; thus, the assumption made earlier that $\delta^*/\theta = 2.554$ is valid.

3.2 Comparison of Theoretical and Experimental Discharge Coefficients

The test results presented in this section also used air at room temperature (24°C) as the working fluid.

Figures 14 through 17 compare theory and experiment for discharge coefficients of various geometries of nozzles. The agreement is best by far in figure 14, which shows that the one-dimensional assumptions for the flow velocities are good in smoothly converging nozzles. In figure 15, while the agreement is fairly good, the process by which the nozzle was made (photo-etched Dycril plastic) may be causing the discrepancies. Figure 16 shows the same trends as figure 17, in that the theory underestimates c_d slightly at the low Reynolds numbers and slightly overestimates c_d at the higher ones. The overall agreement is quite good in all cases. The discharge coefficient is determined experimentally by measuring the actual flow rate through the nozzle, the

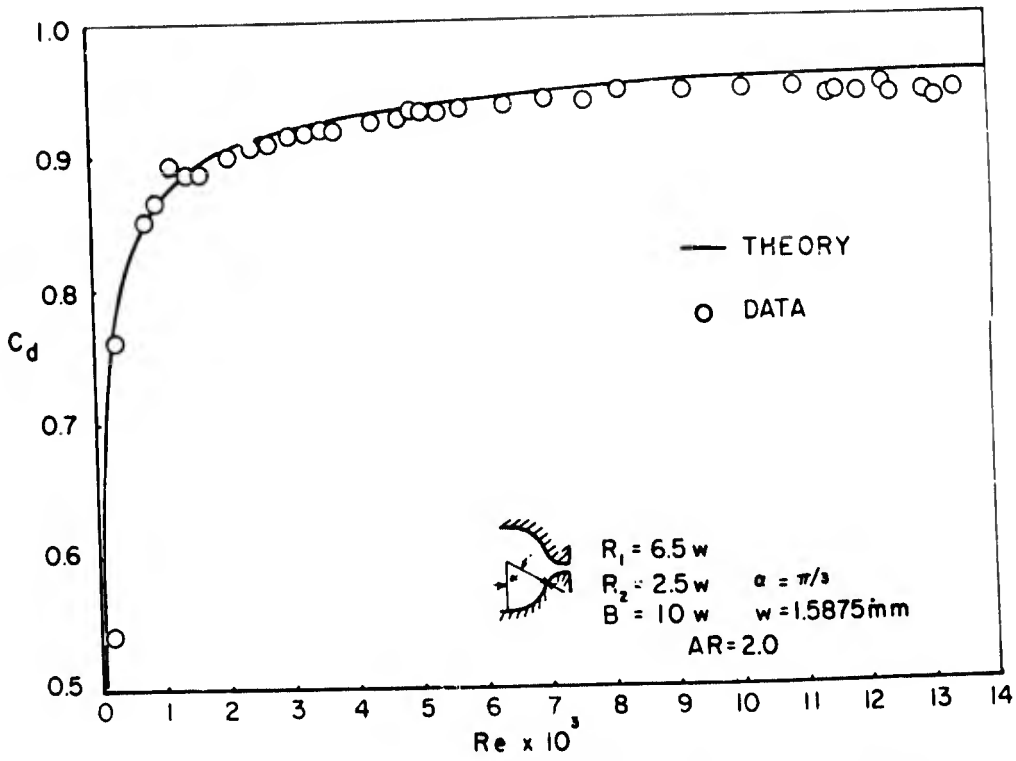

Figure 14. Discharge coefficient versus Reynolds number for a smooth double-arc-of-a-circle nozzle.

actual pressure difference across the nozzle, and the actual cross section of the nozzle exit, and then using equation 2. Equation 2 is used to derive the error in calculating c_d, $\epsilon(c_d)$, as a function of the relative error for the various terms. Assuming that the individual errors are normally distributed so that the standard deviation of the errors of c_d can be assumed the expected error for c_d, then

$$\frac{\epsilon(c_d)}{c_d} = \sqrt{\left[\frac{\epsilon(Q)}{Q}\right]^2 + \left[\frac{\epsilon(A)}{A}\right]^2 + \left[\frac{1}{2}\,\frac{\epsilon(\Delta p)}{\Delta p}\right]^2 + \left[\frac{1}{2}\,\frac{\epsilon(\rho)}{\rho}\right]^2} \qquad (22)$$

Approximate expected errors are: flow measurement, 3 percent (which includes the error of the flowmeter and the reading of the flowmeter output); measurement of a linear dimension, whose size is about 0.5 mm, 1 percent; use of the value of density at 20°C instead of actual room or operating temperature 1 percent; measurement of the pressure difference 3 percent (which includes the gage,

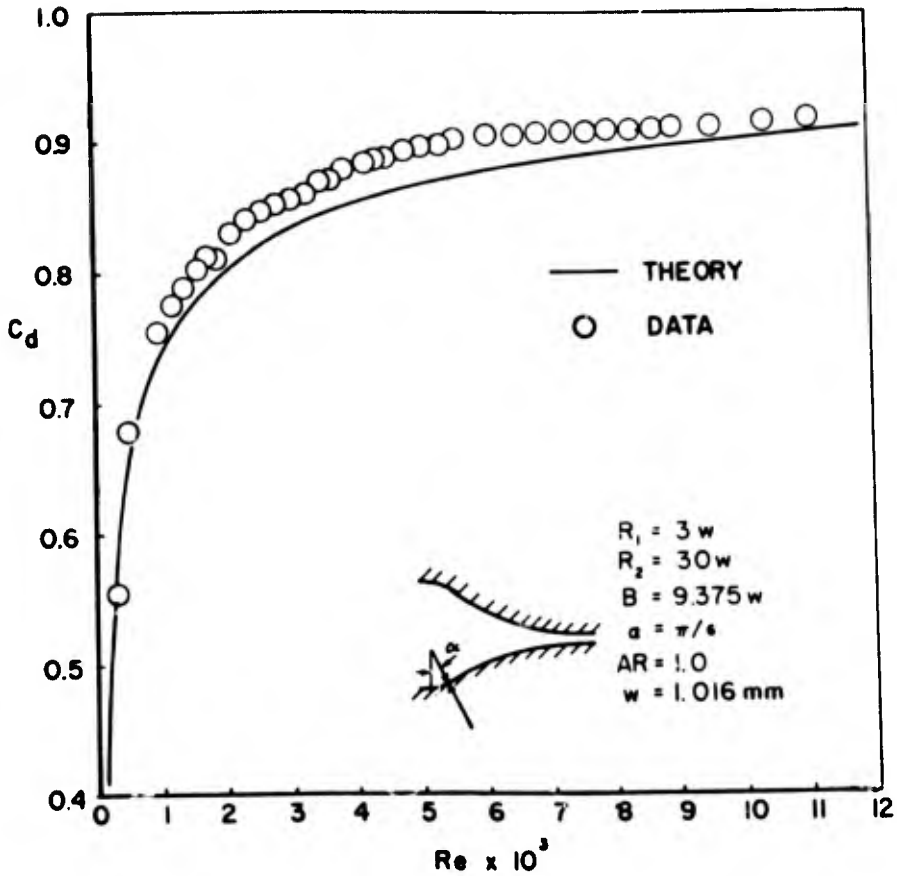

Figure 15. Discharge coefficient versus Reynolds number for a smooth, slender double-arc-of-a-circle nozzle.

transducer, and reading error); and therefore the standard deviation or expected error is about 4.0 percent. If the error in measuring the area is as much as 8 percent, the maximum error could be as high as 10 percent. This critical measurement of area may be important when, due to manufacture, the nozzle exit cross section takes on shapes as shown in figure 18. Following figure 18 are typical reasons for such cross sections.

Taking the value of 4.0 percent as the error expected, the theory agrees very well with all the data, since in the range of applicability of the theory the deviation is never more than 4 percent. It should be noted, however, that even at the low Reynolds numbers the agreement is quite good; thus, there should be some confidence in using the theory over the entire range of Reynolds numbers.

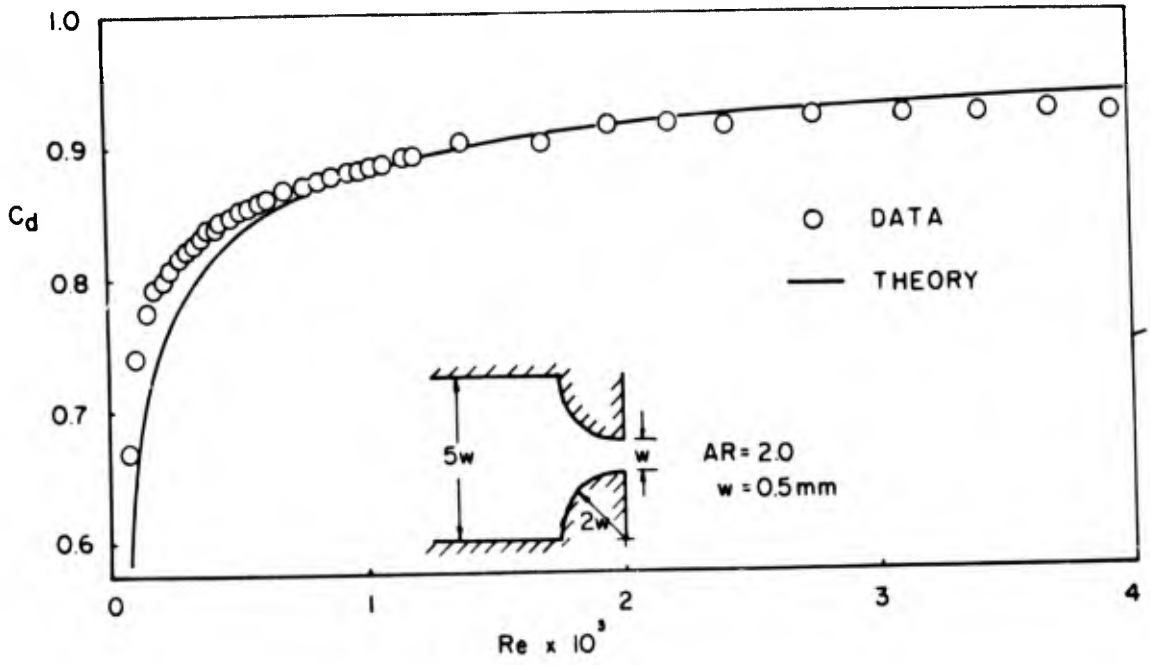

Figure 16. Discharge coefficient versus Reynolds number for a single radius-of-curvature nozzle – small radius.

3.3 Transition to Turbulence and Turbulent c_d

A nozzle with w = 2 mm, an aspect ratio of 3, and a geometry as shown in figure 19 was fed with air by a long round tube of 5-mm ID perpendicular to the plenum (perpendicular to the parallel top and bottom plates). The discharge coefficient determined for the laminar flow (from equations 9, 12, and 13) agrees well at the low end as can be seen in figure 19. The critical Reynolds number Re_q determined from equation 21 was 1945 and the corresponding theoretical laminar c_d at Re_q = 1945 was found to be 0.89. This value, c_d = 0.89, is then assumed to be constant throughout the turbulent region. A hot-film probe flush mounted at the nozzle exit indicated that the flow did indeed become turbulent when $Re_q \simeq 2000$. The agreement between theory and experiment is excellent, as shown in figure 19. Note that the tube diameter to nozzle height ratio d/h in the previous discharge coefficient tests was quite high (over 4), so that transition did not occur in the Reynolds number ranges tested.

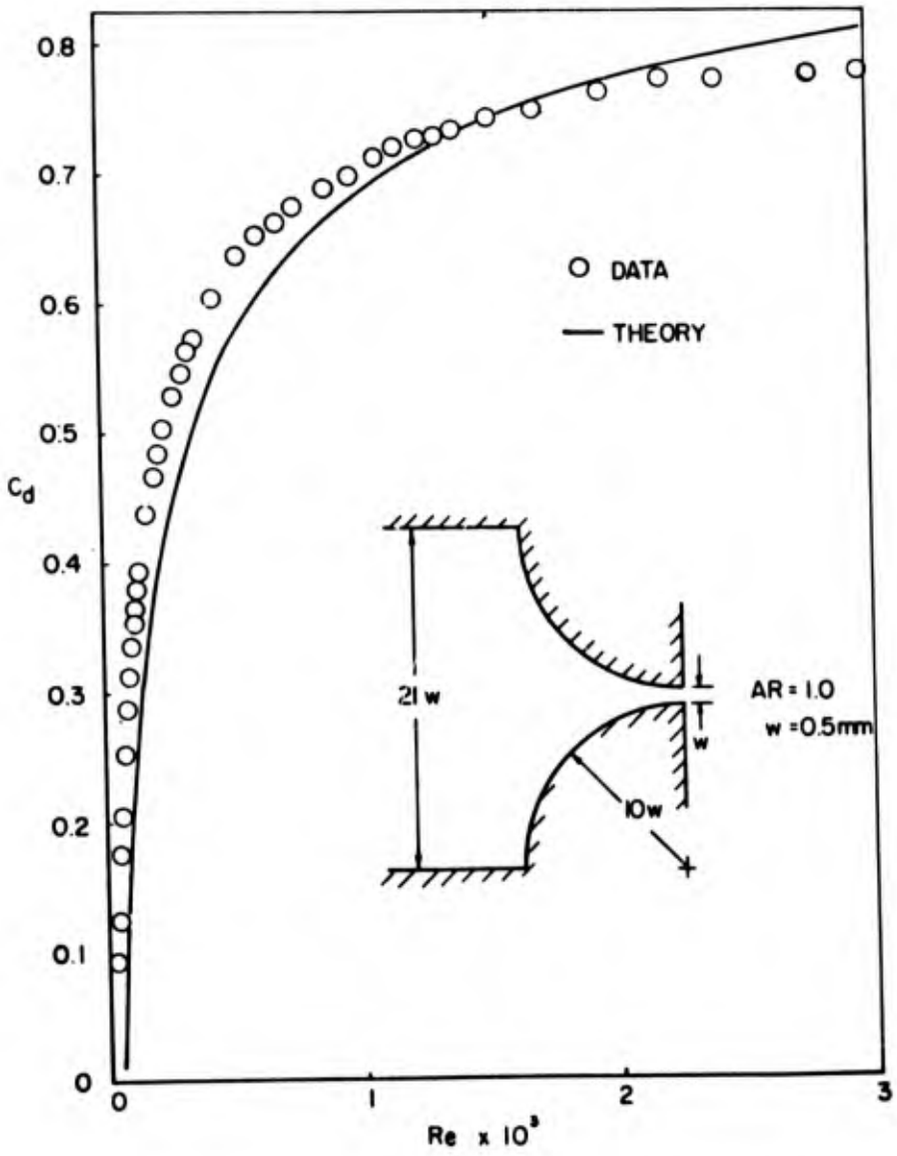

Figure 17. Discharge coefficient versus Reynolds number for a single radius-of-curvature nozzle – large radius.

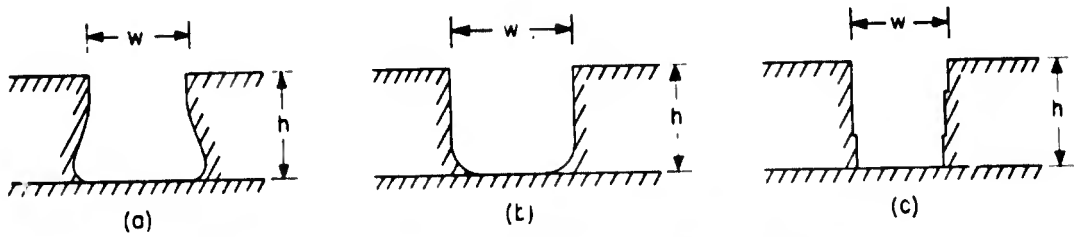

Figure 18. Typical nozzle exit cross-sectional areas.

For figure 18a: Undercutting in an etching process;

18b: Not enough etching, too much round on a mold or stamp;

18c: Uneven pressure on various passes in pantograph milling process.

Considering the small size of the nozzles, large errors can be expected if the tolerances are 0.025 mm (0.001 in.).

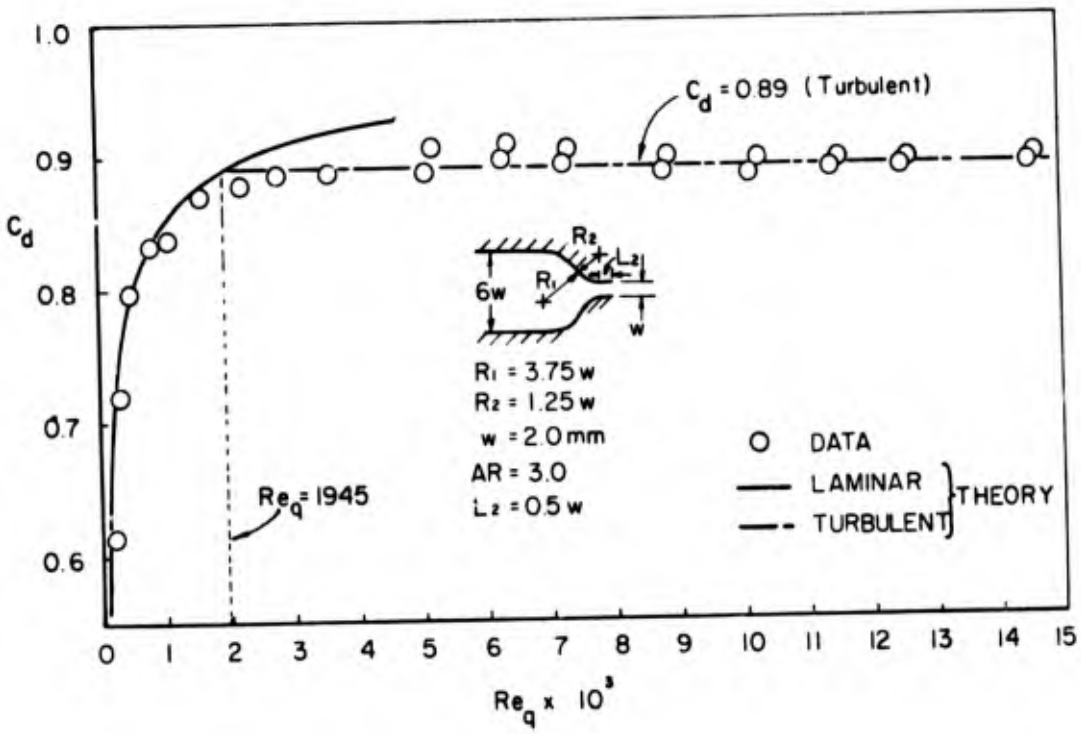

Figure 19. Discharge coefficient versus Reynolds number for a smooth double-arc-of-a-circle nozzle with transition to turbulence.

4. DESIGN CURVES OF c_d VERSUS Re FOR VARIOUS GEOMETRIES

Equations 9, 12, and 13 were combined and solved for various geometries to show the effects of changing some of the parameters. Figure 20 shows the effect of changing the aspect ratio. The discharge coefficient decreases with aspect ratio (equation 9), because viscous effects are greatest near the walls. Figure 21 shows the strong dependence of the discharge coefficient on the amount of throat straight section following the convergence. In this case, c_d decreases with increasing length of straight section, as expected. Figure 22 shows the effect of contraction ratio. At high contraction ratios the effect of change is small, whereas it is most significant when values of the contraction ratio are less than 5.0. In general, c_d decreases with contraction ratio as expected because the viscous forces act for a longer time on a less accelerated fluid.

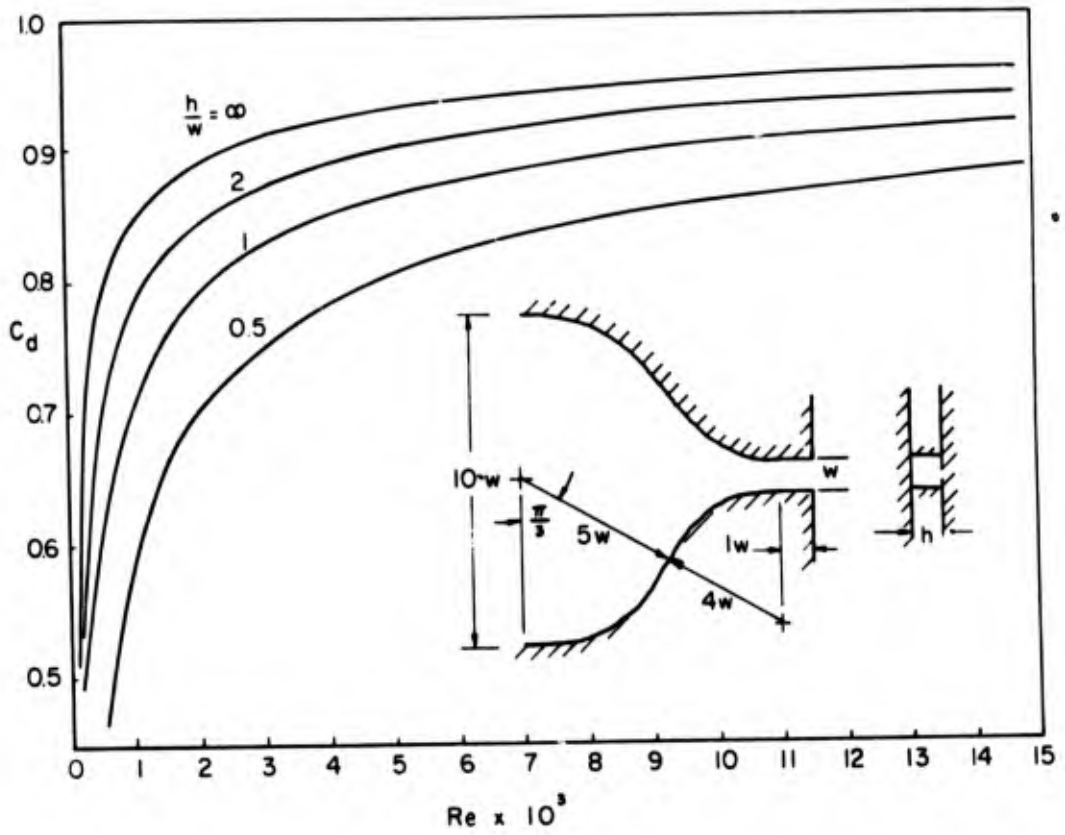

Figure 20. Theoretical discharge coefficient versus Reynolds number – effect of aspect ratio.

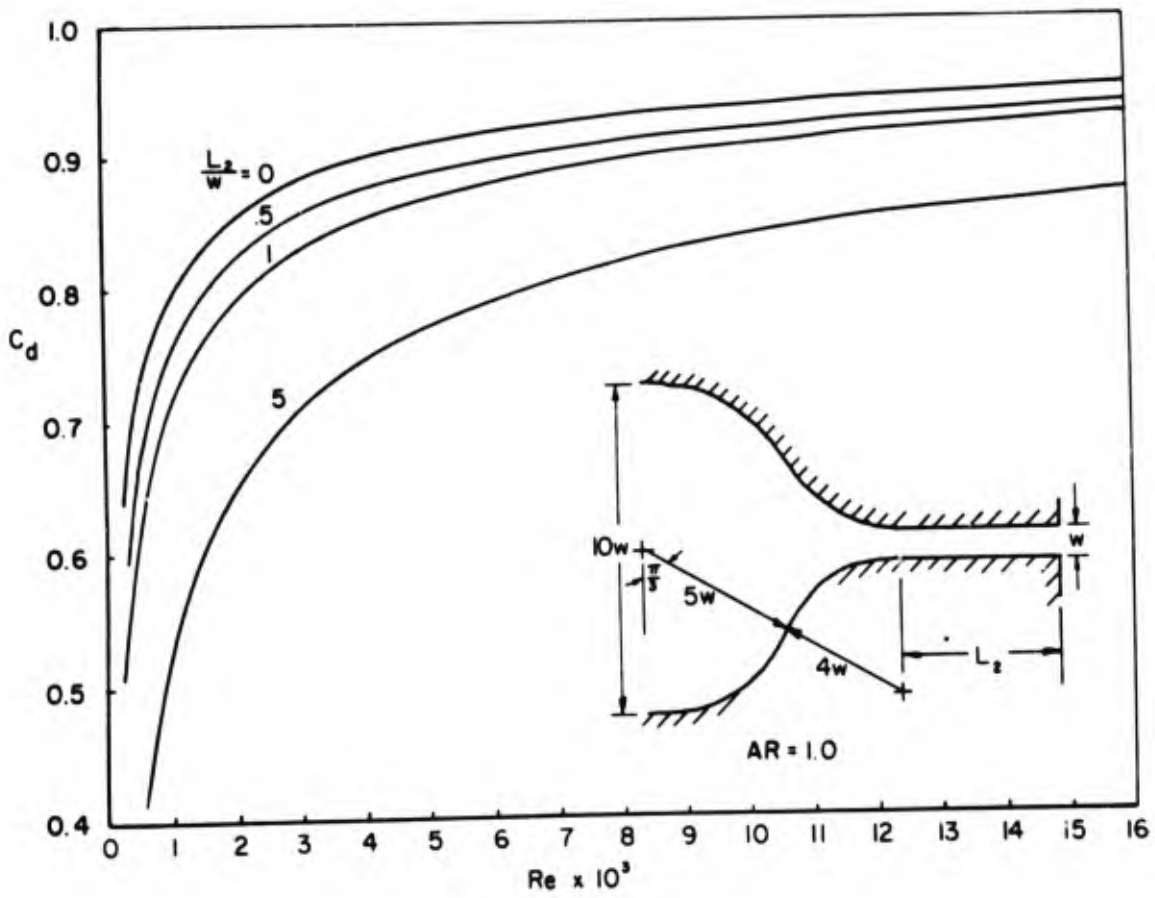

Figure 21. Theoretical discharge coefficient versus Reynolds number – effect of throat straight section.

The effect of altering the various radii for one particular aspect ratio, one contraction ratio, and one length over which the contraction occurs, is very small when the ratio of the radii is within 10; that is, R_1/R_2 or $R_2/R_1 < 10.0$ and $\alpha \leq 1.3$ rad.

5. DISCUSSION AND DESIGN GUIDELINES

In general, the findings herein show that simple 1- or 2-dimensional inviscid flow fields can be used to describe the free-stream flow in a nozzle; and that by using these distributions, results are obtained for the discharge coefficient that are well within experimental tolerances. Furthermore, the inlet conditions to the plenum of a nozzle can determine the onset of turbulence, and

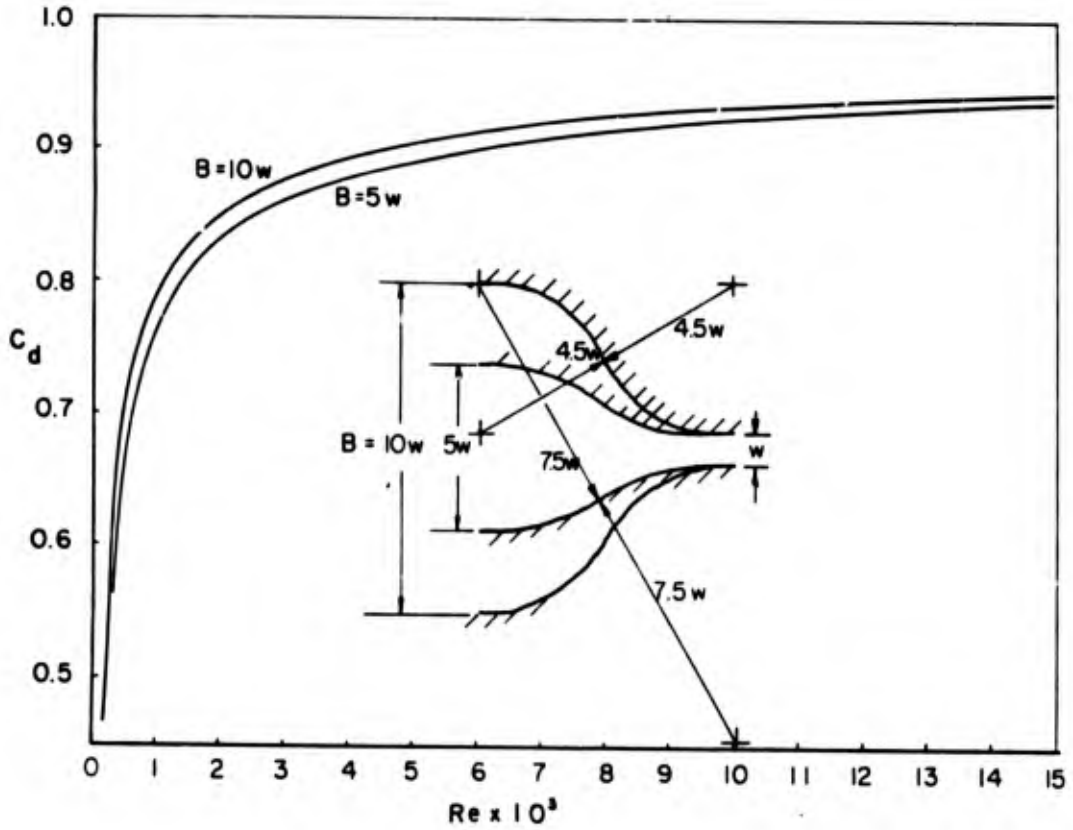

Figure 22. Theoretical discharge coefficient versus Reynolds number – effect of contraction ratio.

a simple relation based on fully developed pipe flow can accurately predict the transition point of a nozzle flow. Turbulent nozzle flow is characterized by a discharge coefficient that is constant from the critical Reynolds number up to at least 2×10^4, well above the normal operating range of fluid amplifiers. The theory has been verified for geometries having nozzle widths of 0.5 mm to 2.0 mm, and, as long as the flow is basically laminar, there is no need to impose any size restrictions on the theory.

From a design standpoint, if the highest possible c_d with the least variation is desired, the following guidelines should be used.

a. Use an aspect ratio greater than one.

b. Use a short (or no) straight section after the convergence.

c. Use a contraction ratio greater than 5.

d. Use a contraction length of about 10 nozzle widths.

Caution must be exercised, however, in using these guidelines. If a large apsect ratio is not feasible, 2.0 is sufficient in most fluid amplifier designs. The use of too high a contraction ratio with too short a contraction length may result in an orifice-like characteristic that causes a vena contracta and a reduced or even decreasing c_d at higher Reynolds numbers. This kind of characteristic exhibits a maximum c_d at Re $\simeq 10^3$ and then a rapid falloff. A good rule of thumb is to make the contraction ratio roughly equal to the contraction length. For example, a planar nozzle having an aspect ratio of two, a zero to one-half nozzle width straight section, a contraction ratio and length of ten, and a ratio of first to second curvatures not exceeding 10 (AR 2, L_2/w 0-0.5, B/w = 10, C. L. = 10 R_1/R_2 or $R_2/R_1 \leq 10$) will have a characteristic so that for Re > 600, $c_d > 0.8$ and for Re > 2500, $c_d > 0.9$.

A high discharge coefficient is not entirely desirable when the aim is to reduce free-stream turbulence. In this case, a fully developed profile may be desired, and, although this flow may become turbulent at a low Re, there is good damping of upstream disturbances so long as it is laminar. Owczarek and Rockwell[7] indicate that the single radius of curvature nozzle (fig. 7) has the highest free-stream turbulence characteristic. It should be noted, however, that they had a very large model, and that disturbances could have been propagated easily since the scale of the turbulence would be much smaller than that of the large dimensions used. This is probably not the case in the small (0.5 mm) fluidic nozzles where the wall interactions and viscous effects tend to reduce the level of turbulence throughout. This point should be carefully considered when scaling. As long as the flow is laminar, the discharge coefficient is independent of size; however, if the dimensions are made too large and free-stream turbulence begins to play a large part, then scaling must be considered in terms of the turbulent micro-scale as well as the physical dimensions of the device.

In general, then, a smooth, continuous nozzle gives the most desirable characteristics. The difference between the discharge coefficient of a nozzle formed by matched circular arcs (fig. 6) or of a beam deflection (lofted) nozzle of the same overall dimensions is negligible. A beam-deflection nozzle can be viewed as a converging section made up of a beam with parallel ends that have been displaced. Van Tilberg et al[8] show this type of nozzle. From a design standpoint, it is generally easier to draw and describe arcs of a circle rather than to plot point by point a polynomial function as in the beam-deflection case. Since fluidic nozzles are manufactured by techniques that require a drawing, the use of the beam-deflection nozzle design becomes tedious and academic.

---

[7]Owczarek, J. and D. Rockwell, "An Experimental Study of Flows in Planar Nozzles," ASME Paper No. 72-Flcs-2, presented at 14th Annual Fluids Engineering Conference, San Francisco, CA, March 1972

[8]Van Tilburg, R.W., R.H. Bellman, and W.L. Cochran, "Fluerics 21. Optical Fabrication of Fluid Amplifiers and Circuits," Harry Diamond Laboratories, Washington, D.C., May 1966

It should be mentioned that in terms of the head loss coefficient, K_L, often used in hydraulics, the discharge coefficient can be written

$$c_d \quad \left[\frac{1}{1 + K_L}\right]^{1/2}$$

This description can be an advantage when considering geometries other than nozzles, such as variable cross-section ducts. In such cases, however, a prior knowledge of the pressure gradient is needed so that the shape factor, Λ, can be calculated to determine the displacement thickness.

In closing, a simple method of calculating nozzle discharge coefficients has been presented utilizing one- and two-dimensional flow fields. Guidelines have been set forth for designing the nozzle with the best discharge coefficient characteristics for a particular application.

6. LITERATURE CITED

1. FLUID METERS, Their Theory and Application, Report of ASME Research Committee on Fluid Meters, 5th edition, 1959

2. Simmons, F.S., "Analytic Determination of the Discharge Coefficients of Flow Nozzles," NACA TN 3447, Lewis Flight Propulsion Labs, Cleveland, Ohio, April 1955

3. Williams, J.C. and F.O. Smetana, "Theoretical Study of a Convergent Nozzle and Free Jet Flow," Proceedings of the Fluid Amplification Symposium, Harry Diamond Laboratories, Vol. 1, October 1965

4. McRee, D.I., "Experimental Study of a Convergent Nozzle and Free Jet Flow," Proceedings of the Fluid Amplification Symposium, Harry Diamond Laboratories, Vol. 1, October 1965

5. McRee, D.I. and H.L. Moses, "The Effect of Aspect Ratio and Offset on Nozzle Flow and Jet Reattachment," Advances in Fluidics, edited by F.T. Brown, presented at 1967 ASME Fluidics Symposium, Chicago, Illinois, May 1967

6. Schlichting, H., Boundary Layer Theory, McGraw-Hill, N. Y., 4th edition, 1960, pp 122, 244, 247, 251, 413

7. Owczarek, J. and D. Rockwell, "An Experimental Study of Flows in Planar Nozzles," ASME Paper No. 72-Flcs-2, presented at 14th Annual Fluids Engineering Conference, San Francisco, California, March 1972

8. Van Tilberg, R.W., R.H. Bellman, and W.L. Cochran, "Fluerics 21. Optical Fabrication of Fluid Amplifiers and Circuits," Harry Diamond Laboratories, Washington, D.C., May 1966